Research Paper

Low-Redshift Observational Constraints on Dark Energy Cosmologies

Mohammad Malekjani

Department of Physics, Bu-Ali Sina University, Hamedan 65178, 016016, Iran;
email: malekjani@basu.ac.ir

Abstract. Applying the Markov chain Monte Carlo algorithm and using low-redshift observational data, we put cosmological constraints on dark energy cosmologies. Our main aim is to show the influence of each data sample on the procedure of constraining. The main results of our analysis are as follows. In the case of the Pantheon catalog of supernovae, one can put approximately three times tighter constraints on the cosmological parameters compare to the early Gold dataset. Combining the Pantheon with the Hubble data, we obtain ~ 1.5 times tighter constraints compare to the Pantheon solely. We show that in cluster scale due to low growth rate data with large error bars, one cannot put tight constraints on the cosmological parameters. Combining the expansion and growth rate data leads to tighter constraints on the cosmological parameters. While the local value of Hubble constant H_0 has a $\sim 3.4\sigma$ tension with Planck inferred result, we show that by combining the expansion and growth data with local H_0 data, the tension is alleviated to a 1.7σ. Finally, jointing the Pantheon, Hubble data, growth rate, H_0 with the BAO measurements gets roughly $7 - 8\%$ tighter constraints on the matter density and Hubble constant parameters.

Keywords: Cosmology: Theory, Cosmology: Dark energy, Observational data

1 Introduction

Analysis of the various observational data including those of the supernovae type Ia (SnIa) [1–4], cosmic microwave background (CMB) [5–7], baryonic acoustic oscillation (BAO) [8] and the large scale structure (LSS) [9–11] indicate that the current universe experiences an accelerated expansion. From the viewpoint of SnIa, cosmologists use the observed light curves and redshifts of SnIa to measure the cosmological parameters. SnIa is the standard candle of cosmology because it is very luminous and very standardized [12,13]. Using the definition of apparent and absolute magnitudes and calling the Hubble parameter from the cosmological model, one can calculate the theoretical value of the distance modulus in terms of redshift and compare it with the observational value. It has been shown that the predicted value of the distance modulus in the matter-dominant universe for redshifts above $z \sim 0.5$ is less than the observational values [4]. To resolve this problem, one of the easiest and possible solutions is adding the cosmological constant Λ to the energy budget of the universe [14]. In this case, the cosmic acceleration of the universe changes from the

decelerated to accelerated phase. In addition to Λ, the dynamical models of dark energy (DE) with evolving equation of state (EoS) parameter can also eliminate the incompatibility between the results of observations and theory [15]. It is interesting to mention that from the total energy density of the universe, only $\sim 30\%$ consists of the luminous and dark matter, while the rest corresponds to DE. Despite a lot of studies on DE, its physical properties, origin, and nature are yet unknown. The simplest candidate for DE is the cosmological constant with constant EoS parameter equal to -1. But there is a discrepancy of some 120 orders of magnitude between the theoretical and observational values of the energy density of DE known as the fine-tuning problem [15,16]. Also, the cosmological constant Λ suffers from the cosmic coincidence problem [15,16]. These two problems can be solved or at least alleviated in the context of dynamical DE models [17]. As was mentioned above, in dynamical DE models, the EoS parameter differs from -1 and can vary with cosmic redshift. In this work, using the latest low-redshift observational data including those of SnIa, cosmic chronometers (CC) data (see Table 1), BAO measurements (See Tables 3 and 4), local measurement on Hubble constant H_0 and the growth rate data from redshift space distortion (RSD) (see Table 2), we obtain the observational constraints on the properties of DE. To do this, we assume the concordance ΛCDM and wCDM cosmologies. In later model, we adopt the constant EoS parameter of DE differs from -1 and smaller than $-1/3$ [17]. We also use the different catalogs of SnIa data to show that how much we put tighter constraints on the cosmological parameters by increasing the observational data points of SnIa at higher redshifts. The SNIa catalogs used in this work are: (i) the Gold sample (141 distinct SnIa data points) [18–20], (ii) Union2.1 (570 data SnIa data points) [21] and (iii) Pantheon sample (1048 data points) [22]. Notice that constraining the well-konwn ΛCDM and wCDM model using the low-redshift observations has been widely investigated. However, the novelty of our analysis can be stated as follows. For the first time, we compare the results of using different catalogs of Supernova data including early Gold sample to recent Pantheon one. We explicitly show that how much one gets better constraints on cosmological parameters when uses the Pantheon catalog compare to previous catalogs. In the next step, we combine the Pantheon sample with other low redshifts observational data such as the Hubble rate and RSD data, step by step. In each step, we show that how much one gets better results quantitatively. Notice that in many similar studies, the results of all combined observational data are presented, for example, see [23,25–30] an references therein. We calculate the precision of our measurement on the cosmological parameters when we add the observational dataset to the previous ones. Moreover, we compare the results of our analysis with and without local H_0 data point with CMB value from Planck results. While the local value of Hubble constant H_0 has a big tension with Planck inferred value, we can alleviate the tension based on the analysis which uses the combined the local H_0 data to the other low-redshift observations. Finally, by adding the BAO data point to other datasets, we get roughly $7 - 8\%$ tighter bounds on matter energy density Ω_{m0} and Hubble constant h. In overall, we emphasize that our step by step MCMC analysis can show the role of each observational dataset on the constraining the DE properties.

We organize the paper as follows. In Section (2), we present the DE models considered in this work. In Section (3), we present the low-redshift observational data including those of SnIa, CC, BAO and RSD data used in our analysis. In Section (4), the results of observational constraints based on the SnIa, CC and RSD data are presented. In Section (5), we combine the low-redshift observational data used in Section (4) with the local H_0 and BAO data to see the impact of these experiments on our results. Finally, we conclude this work in Section (6).

2   DE models

As was mentioned in introduction, our aim in this work is to study the influence of each data sample on the constraining of the cosmological parameters. So, we consider two simple and relevant ΛCDM and wCDM cosmological models. Here, we present the Hubble expansion for DE models used in this work. In the case of wCDM model, one assumes that the EoS parameter of DE is constant and less than $-1/3$. In this model, the Hubble parameter in the flat low-redshift universe reads [15]

$$E^2(z) = H^2/H_0^2 = \Omega_{m0}(1+z)^3 + (1-\Omega_{m0})(1+z)^{3(1+w_{de})}, \tag{1}$$

where Ω_{m0} is the current value of dimensionless energy density of non-relativistic matter, w_{de} is the EoS parameter of DE and z is the cosmic redshift parameter. Notice that in the low-redshift universe, we can ignore the contribution of radiation in the total energy budget of the universe. In standard ΛCDM cosmology, the Hubble parameter in low redshift universe simply reads

$$E^2(z) = \Omega_{m0}(1+z)^3 + (1-\Omega_{m0}), \tag{2}$$

In the limiting case of Einstein- de Sitter universe (EdS), the Hubble parameter in low-redshift flat cosmology simply reads $E^2(z) = (1+z)^3$. In the next section, using the low-redshift observational data and in the context of the current cosmological models, we study the properties of DE in both expansion and perturbation levels.

3   Low redshift observational data

In this section, we introduce different low-redshift observational data used to put constraints on DE properties. At the expansion level, we use different catalogs of SnIa data, CC data, BAO measurements and local value of Hubble constant H_0. At the perturbation level, we use the RSD data obtained from the redshift space distortion of galaxy clusters. In fact, the RSD data can help us to study the behavior of DE in small scales where the impact of DE on the growth of cosmic structures will be significant.

3.1   Supernova type Ia

The observations of distant SnIa at the last two decades cause a big revolution in modern cosmology. SnIa is one of the most important objects in observational cosmology because of their role as distance indicators. It is bright enough to observe at high redshifts and has a uniform peak luminosity. SnIa is expected to evolve less compared to other objects such as galaxies. In many studies, SnIa has been used as a distance indicator in order to show the accelerating expansion of the universe [4]. Cosmologists use the observed light curves and redshifts of SnIa to put constraints on the cosmological models. Given the apparent and absolute magnitude, the distance modulus of supernova can be written in the form of

$$\mu(z) = 5\log\left((1+z)\int_0^z \frac{dz}{E(z)}\right) + \mu_0, \tag{3}$$

where $\mu_0 = 42.38 - 5\log h$ and h is the current value of Hubble constant H_0, in units of $100 km/s/Mpc$. By inserting $E(z)$ from the cosmological models in equations (1 and 2), we show the redshift evolution of the residuals of distance modulus computed for EdS and wCDM universes with respect to standard ΛCDM cosmology and then compare it with the

Table 1: Hubble data extracted from different cosmic chronometers used in the current study.

z	$H(z)$	σ_H	Reference
0.070	69.0	19.6	[31]
0.100	69.0	12.0	[32]
0.12	68.6	26.2	[31]
0.17	83.0	8.0	[32]
0.179	75.0	4.0	[33]
0.199	75.0	5.0	[33]
0.2	72.9	29.6	[31]
0.27	77.0	14.	[32]
0.28	88.8	36.6	[31]
0.35	76.3	5.6	[34]
0.352	83.0	14.0	[33]
0.4	95.0	17.0	[32]
0.48	97.0	62.0	[35]
0.593	104.0	13.0	[33]
0.68	92.0	8.0	[33]
0.781	105.0	12.	[33]
0.875	125.0	17.0	[33]
0.88	90.0	40.0	[35]
0.9	117.0	23.0	[32]
1.037	154.0	20.0	[33]
1.3	168.0	17.0	[32]
1.43	177.0	18.0	[32]
1.53	140.0	14.0	[32]
1.75	202.0	40.0	[32]
2.3	224.0	8.0	[36]

Table 2: The growth rate data extracted from redshift space distortion [37].

z	$f\sigma_8(z)$	$\sigma_{f\sigma_8}$
0.02	0.428	0.0465
0.02	0.398	0.065
0.02	0.314	0.048
0.10	0.370	0.130
0.18	0.360	0.090
0.38	0.440	0.060
0.25	0.3512	0.058
0.37	0.4602	0.0378
0.32	0.384	0.095
0.59	0.488	0.060
0.44	0.413	0.080
0.60	0.390	0.063
0.73	0.437	0.072
0.60	0.550	0.120
0.86	0.400	0.110
1.40	0.482	0.116

Table 3: BAO dataset in old format.

Survey	z	d	σ	reference
6dFGS	0.106	0.336	0.015	[38]
SDSS-LRG	0.35	0.1126	0.0022	[39]

Table 4: BAO dataset in new format.

Survey	z	α^* (Mpc)	σ (Mpc)	r_s^{fid} (Mpc)	
BOSS-MGS	0.15	664	25	148.69	[40]
BOSS-LOWZ	0.32	1264	25	149.28	[41]
WiggleZ	0.44	1716	83	148.6	[42]
	0.6	2221	101	148.6	
	0.73	2516	86	148.6	
BOSS-CMASS	0.57	2056	20	149.28	[41]
BOSS-DR12	0.38	1477	16	147.78	[43]
	0.51	1877	19	147.78	
	0.61	2140	22	147.78	

observational data in Figure (1). Notice that here we fix the current value of matter density Ω_{m0} and also fix the Hubble parameter h based on the results presented in Table (6). We simply see that the distance modulus in Einstein de-Sitter (EdS) universe without invoking of DE (e.g., $\Omega_m = 1$) is deviated from the observational data at relatively high redshifts (e.g., $z > 0.5$). While in wCDM and concordance ΛCDM universes, the theoretical prediction of distance modulus is well fitted to observations. Here the observational data are chosen from the Pantheon catalog, where we use the corrected heliocentric redshifts updated by [22].
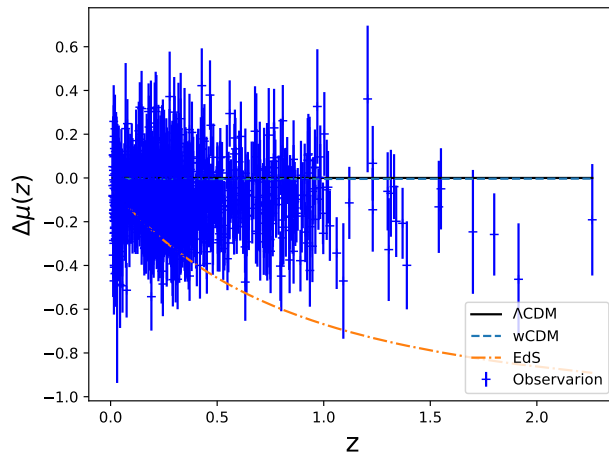
Figure 1: The redshift evolution of the residuals of distance modulus computed for the cosmological models: wCDM and EdS universe with respect to standard ΛCDM Universe. The EdS model deviates from the observational data at higher redshifts while other models are well fitted to observations equally as standard model. The observational data showed here are from the Union Pantheon catalog [22].

3.2 CC data

The other observational sample used here are the Hubble data which include the value of Hubble parameter, H(z), obtained from CCs at different redshifts. The independent measurements of CC data at different redshifts with their errors and references are collected in Table (1). Theoretically, it is very easy to obtain the Hubble parameter at any cosmic redshift. In fact, $H(z) = H_0 E(z)$ where $E(z)$ is given by equations (1 and 2), respectively, for wCDM and ΛCDM models and $H_0 = 100h$ is the Hubble constant. In Figure (2), we show the evolution of the Hubble parameter calculated for our cosmological models in this work as well as the observational data given in Table (6). Notice that we fix Ω_m and h based on their values in Table (5). For comparison, we also plot the Hubble parameter in the context of EdS model. We see that the Hubble parameter in the EdS universe deviates from the observational data. While wCDM and concordance ΛCDM models fit the observations.

3.3 RSD data

The data from SnIa catalogs and CC sample are geometrical because they are directly related to cosmic distance. In other words, these experiments are valuable when we study
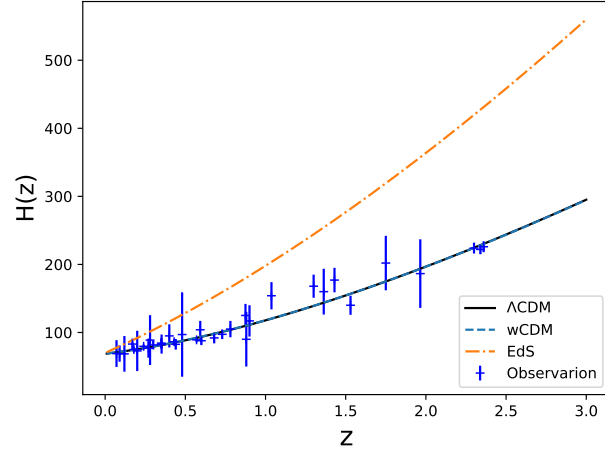
Figure 2: The redshift evolution of the Hubble parameter for cosmological models: wCDM, ΛCDM, and EdS universe. The EdS universe deviates from the observational data while other models fit observations. The CC data points showed here are reported in Table (1).
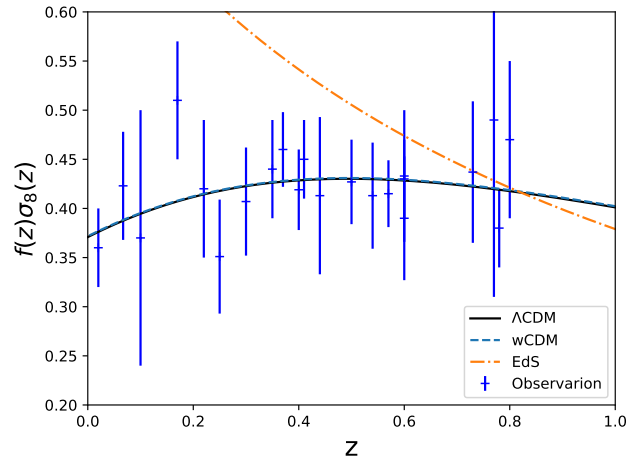

Figure 3: The redshift evolution of $f(z)\sigma_8(z)$ quantity calculated for cosmological models: wCDM, ΛCDM, and EdS universe. As expected, the EdS universe deviates from observational data while other models fit observations. The RSD data points are presented in Table (2).

cosmology at the uniform large scales. However, in smaller scales, the perturbations can grow and the universe is not homogeneous. In fact at scales which are currently smaller than $100h^{-1}Mpc$, the universe is not isotropic and homogeneous. In such scales we can explore how DE can impact on the growth of perturbations? Fortunately, from the observational point of view, cosmologists can extract some important data from RSD of galaxies that are known as $f(z)\sigma_8$ data [44]. Here, $f(z)$ is the growth function of matter perturbations and σ_8 is the mass variance inside the radius of $8h^{-1}Mpc$. We present the updated $f(z)\sigma_8$ data at different redshifts with their errors and references in Table (2). Using the $f(z)\sigma_8$ data, we can study the DE models in the perturbation level and investigate how a given DE model can suppress the growth of matter perturbations. In overall, one can combine all data from background and perturbation levels to study how much a given DE model is consistent with observations. [25,27,28,45]. Also, the RSD data can be used as a probe to study the differences between the growth of perturbations in the modified theory of gravity and general relativity [46]. In addition, using the RSD data, one can compare DE models with the standard ΛCDM cosmology at the level of perturbation. In order to calculate the theoretical value of $f(z)\sigma_8(z)$, we should first compute the linear evolution of matter perturbation δ_m from the following equations [47]

$$\theta' + (\frac{2}{a} + \frac{E'}{E})\theta - \frac{3}{2a^5}\Omega_{m0}\delta_m = 0, \tag{4}$$

$$\delta'_m + \frac{\theta}{a} = 0, \tag{5}$$

where θ is the divergence of the peculiar velocity of perturbations and prime is the derivative with respect to the scale factor a. To solve the above equations, we adopt the following adiabatic initial conditions at the initial scale factor $a_i = 10^{-4}$ [27,28,48]

$$\delta_{mi} = 1.2 \times 10^{-5}, \delta'_{mi} = \frac{\delta_{mi}}{a_i}. \tag{6}$$

The initial scale factor $a_i = 10^{-4}$ refers the end of radiation dominated phase meaning that at this scale factor the universe enters the matter dominated era. By choosing the above value for δ_{mi} at $a_i = 10^{-4}$, we guaranty that the matter perturbation can not grow to the non-linear regimes and remains in a linear phase ($\delta_m << 1$). We can simply calculate the redshift evolution of the growth function $f(z) = \frac{d\ln\delta_m}{d\ln a}$ on the basis of the following equation

$$f(z) = -\frac{1+z}{\delta_m(z)}\frac{d\delta_m(z)}{dz}. \tag{7}$$

Since the evolution of the mass variance $\sigma_8(z)$ is similar to that of the matter perturbation δ_m, we can write the following relation

$$\sigma_8(z) = D(z)\sigma_8(z=0), \tag{8}$$

where $D(z) = \frac{\delta_m(z)}{\delta_m(z=0)}$ and $\sigma_8(z=0)$ is the current value of the mass variance inside the sphere with radius $8h^{-1}$Mpc. Also, the present value of the mass variance for a given DE model is related to that of the ΛCDM universe as follows [23,24]

$$\sigma_8(z=0) = \sigma_8^\Lambda(z=0)\frac{\delta_m(z=0)}{\delta_m^\Lambda(z=0)}. \tag{9}$$

Using equations (4, 7, 8 & 9), we compute the $f(z)\sigma_8(z)$ quantity for a given cosmological model and compare it with observations. In Figure (3), we show the redshift evolution

of $f(z)\sigma_8(z)$ for cosmological models considered in this work. The free parameters of the models are fixed based on the values in Table (8). We see that wCDM and concordance ΛCDM models are well fitted to observations while the traditional EdS universe deviates from the observational data. This simple prediction shows that in the context of standard gravity we need DE not only on large scales to interpret the cosmic acceleration but also in small scales to justify the suppression of the growth of perturbations.
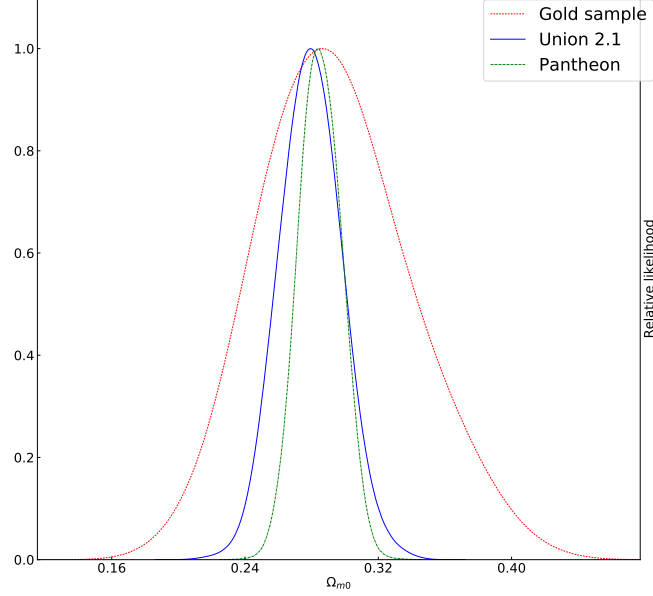
Figure 4: The likelihood function for the energy density of pressureless matter Ω_m obtained from different SnIa catalogs in the context of ΛCDM universe. Using the Pantheon catalog, we obtain tighter constraints compare to other catalogs.

Table 5: Best fit values of the non-relativistic matter density, Ω_{m0}, and EoS parameter of DE, w_{de}, obtained from statistical MCMC analysis using different SnIa catalogs in the context of ΛCDM and wCDM cosmologies.

Model	Ω_{m0}	w_{de}	χ^2_{min}	AIC	Catalog
ΛCDM	$0.294^{+0.041,+0.097,+0.12}_{-0.051,-0.085,-0.11}$	-1.00	167	171	Gold sample
ΛCDM	$0.279^{+0.019,+0.038,+0.052}_{-0.019,-0.036,-0.048}$	-1.00	564	568	Union 2.1
ΛCDM	$0.285^{+0.013,+0.025,+0.033}_{-0.013,-0.025,-0.032}$	-1.00	1037	1041	Pantheon
wCDM	$0.409^{+0.080,+0.12,+0.13}_{-0.032,-0.072,-0.10}$	$-1.58^{+0.17,+0.63,0.79}_{-0.40,-0.44,-0.49}$	163	169	Gold sample
wCDM	$0.280^{+0.078,+0.14,0.16}_{-0.063,-0.15,-0.23}$	$-1.04^{+0.23,+0.39,+0.43}_{-0.16,-0.45,-0.73}$	565	571	Union 2.1
wCDM	$0.347^{+0.039,+0.067,+0.081}_{-0.032,-0.072,-0.10}$	$-1.24^{+0.15,+0.28,+0.33}_{-0.15,-0.29,-0.42}$	1035	1041	Pantheon

3.4 BAO data

The BAO measurements are important data to study the present and future universe. These data are extracted from seven different surveys including 6dFGS, SDSS-LRG, BOSS-MGS,
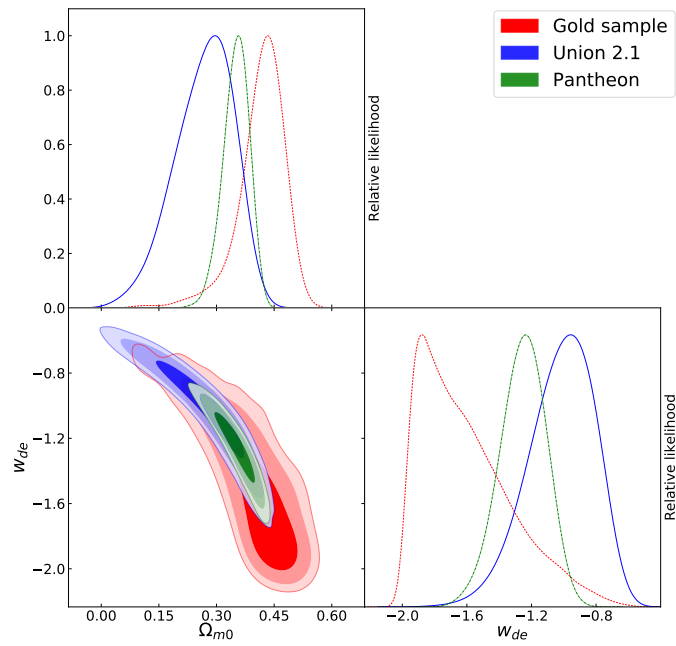
Figure 5: The confidence regions and marginalized likelihood functions for cosmological parameters Ω_{m0} and w_{de} obtained from different SnIa catalogs in the context of wCDM universe. We see that using the Pantheon data, we can put tighter constraints on the cosmological parameters compare to union 2.1 and Gold Sample catalogs.

BOSS-LOWZ, WiggleZ, BOSS-CMASS and BOSS-DR12. These data, errors, and corresponding references are collected in Tables (3) and (4). In Table (3), the quantity $d(z)$ is defined as

$$d(z) = \frac{r_s(z_d)}{D_v(z)}, \tag{10}$$

where $r_s(z_d)$ is the comoving sound horizon at the baryon drag epoch, z_d, which is given by

$$r_s(z_d) = \int_0^a \frac{c_s da}{a^2 H(a)}. \tag{11}$$

Also, the quantity $D_v(z)$ in equation (10) is given as follows

$$D_v(z) = [(1+z)^2 D_A^2(z) \frac{z}{H(z)}]^{\frac{1}{3}}, \tag{12}$$

where $D_A(z)$ is the angular diameter distance. Notice that we adopt the fitting formula for z_d from [49] and also use the following formula for baryon sound speed

$$c_{\rm s}(a) = \frac{1}{\sqrt{3(1 + \frac{3\Omega_b^0}{4\Omega_\gamma^0} a)}}, \tag{13}$$

where we fix the present value of radiation energy density as $\Omega_\gamma^0 = 2.469 \times 10^{-5} h^{-2}$ [50]. Notice that, in Table (4), the quantity α^* is equal to $d^{-1}(z) \times r_s^{fid}$.

3.5 H_0 data point

Recent improvements in the process of measuring the value of Hubble constant H_0 result $H_0 = 73.48^{+1.66}_{-1.66}$ Km/s/Mpc [51]. This measurement increases the tension with respect to the Planck-inferred value, $H_0 = 67.4^{+0.5}_{-0.5}$ Km/s/Mpc [52], to roughly 3.5σ. Recent Gaia DR1 parallax measurements of Cepheids are also confirm the high tension between the local and Planck inferred values of H_0 ([53]). Also, the time-delay cosmography measurements of quasars which pass through the strong lenses is another approach to set the independent constraints on H_0. In this way, the efforts of ([54]) by using three strong lenses result $H_0 = 71.9^{+2.4}_{-3.0}$ Km/s/Mpc in the context of flat ΛCDM model with free parameter of energy density ([55]). Fixing the energy density $\Omega_{\rm m0} = 0.32$ motivated by the Planck results, yields a value $H_0 = 72.8^{+2.4}_{-2.4}$ Km/s/Mpc. These results are in tension with 1.7σ and 2.5σ with the Planck inferred value, while are perfectly consistent with the local measurements of H_0. The above statements motivate us to consider the local value of H_0 as an another low-redshift cosmological data point in our analysis.

4   Observational constraints

In this section, we use both the expansion and RSD data and implement a statistical MCMC analysis for the cosmological models considered in this study. For more details regarding the MCMC technique used in this work, we refer the reader to [23,27–29,50]. The expansion datasets that we use in this analysis include data from SnIa, CC, BAO and local data of H_0. Here we use the SnIa data from three different catalogs including those of Gold sample catalog (157 distinct data points) [18–20], Union 2.1 catalog (570 distinct data points) [21] and Pantheon catalog (1048 data points) [22]. Using three different catalogs of SnIa

sample, we want to show how increasing the data points of SnIa experiments from early Gold sample data to current Pantheon data causes the narrower constraints on the cosmological parameters. In addition to SnIa data, we use the CC data presented in Table (1). In fact, by combining the SnIa data and the data from CC experiments, we can put tighter constraints on the cosmological models. On the other hand, using the RSD data in Table (2) and applying the MCMC analysis, we study the behavior of DE in perturbation level. We put constraints on the cosmological models using the solely RSD data and compare it with that of the expansion level. Finally, combining the data in expansion level (SnIa and CC) with the RSD data and applying the overall MCMC analysis, we put constraints on the cosmological parameters and discuss how combining the above different sets of cosmological data gets the tighter constraints on the cosmological parameters.

4.1   SnIa data

The first dataset that we consider is the SnIa distance modulus from different SnIa samples mentioned above. The chi-square function for a distance modulus of supernova data is given by

$$\chi_S^2 = \sum_{i=1}^{N} \frac{[\mu_{th}(z_i) - \mu_{obs}(z_i)]^2}{\sigma_i^2}, \tag{14}$$

where μ_{th} and μ_{obs} are, respectively, the theoretical and observational values of distance modulus and σ_i is the uncertainties corresponding to observational data. Here N is the number of observational data. Notice that μ_{th} is given by equation (3). In MCMC analysis, using the statistical approach based on the Metropolis-Hastings algorithm [56], we find the confidence levels of the cosmological parameters. We also find the minimum of χ_S^2 for specific values of cosmological parameters in the space parameters. We define a statistical vector p in space parameter containing the cosmological parameters for a given DE model. Notice that before finding the minimum value of χ_S^2, we marginalize the χ_S^2 over the cosmological parameter h appearing in last term of equation (3). Our marginal likelihood analysis have also been used for Gold sample data [57].

Hence, the vector p in ΛCDM cosmology contains only Ω_{m0} as a free parameter and we have $p = \{\Omega_{m0}, w\}$ for wCDM model. The results of MCMC analysis are shown in Figures (4) and (5), respectively, for standard ΛCDM cosmology and wCDM model. Also, the numerical results are presented in Table (5). In the case of ΛCDM model (Figure 4), we see that the constraint on the parameter Ω_{m0} is tighter when we use the Pantheon catalog compare to Gold sample data. We also see that the constraint using Pantheon catalog is tighter than that of the Union 2.1 catalog. Quantitatively speaking, 1σ, 2σ and 3σ uncertainties of Ω_{m0} for Gold sample data are 0.042, 0.0775 and 0.1425, respectively. In the case of Union 2.1 data, these values are 0.021, 0.040 and 0.053, respectively. Finally we have 0.014, 0.027 and 0.035, respectively, for 1σ, 2σ and 3σ errors using the Pantheon catalog. In addition, we calculate the quantity $\frac{1}{\Delta\Omega_{m0}}$ for different 1σ, 2σ and 3σ confidence regions. A large value of $\frac{1}{\Delta\Omega_{m0}}$ means a tighter constraint and our results show that the Pantheon catalog provides a better constraint than both the Union 2.1 and Gold sample catalogs. The quantity $\frac{1}{\Delta\Omega_{m0}}$ calculated within 1σ, 2σ and 3σ confidence regions for Pantheon are respectively ~ 71, ~ 37 and ~ 28. While these values are ~ 47, 25 & ~ 18 for Union 2.1 and ~ 23, ~ 13 & ~ 7 for the Gold sample catalog. In the case of wCDM model (Figure 5), we see that for Pantheon sample the area of confidence levels in $\Omega_{m0} - w_{de}$ plan is much smaller than that of the Gold sample and Union 2.1 catalogs. Hence, using the Pantheon data, we can get more precise measurement of the cosmological parameters Ω_{m0} and w_{de} compare to other Gold sample and Union 2.1 catalogs. Quantitatively speaking, we calculate the
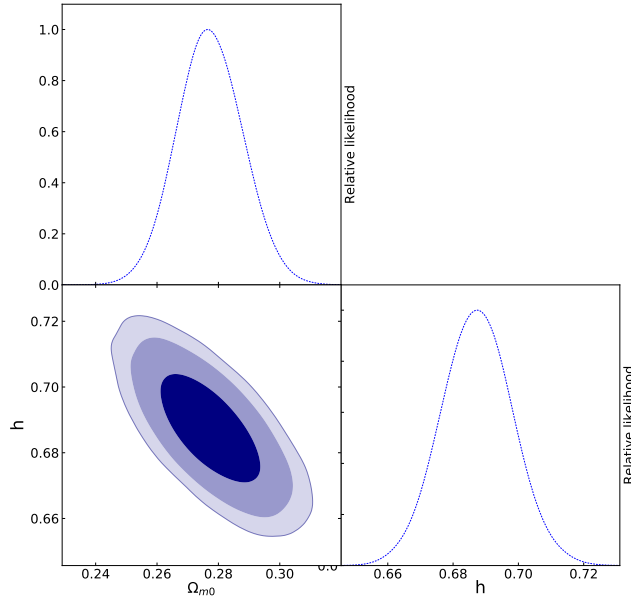
Figure 6: 1σ, 2σ and 3σ confidence regions as well as marginalized likelihood functions in $\Omega_{m0} - h$ plane obtained from the combination of the Pantheon Supernova data and the CC data in ΛCDM cosmology.
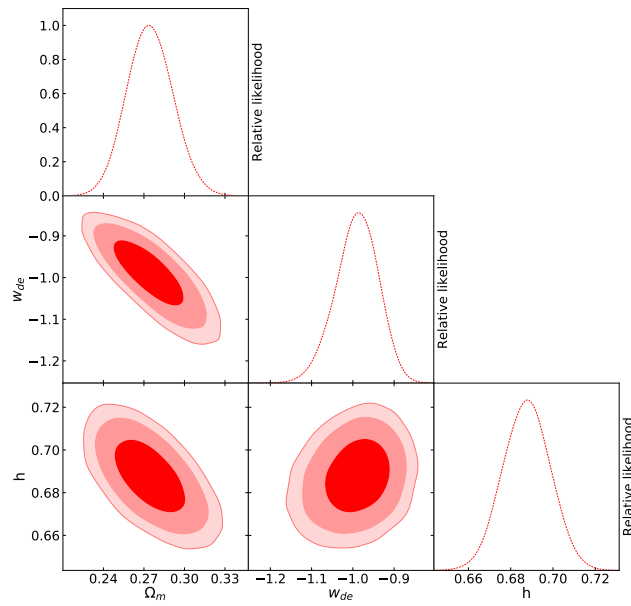

Figure 7: 1σ, 2σ and 3σ confidence regions as well as marginalized likelihood functions for cosmological parameters obtained from the combination of the Pantheon Supernova data and the CC data in wCDM cosmology.
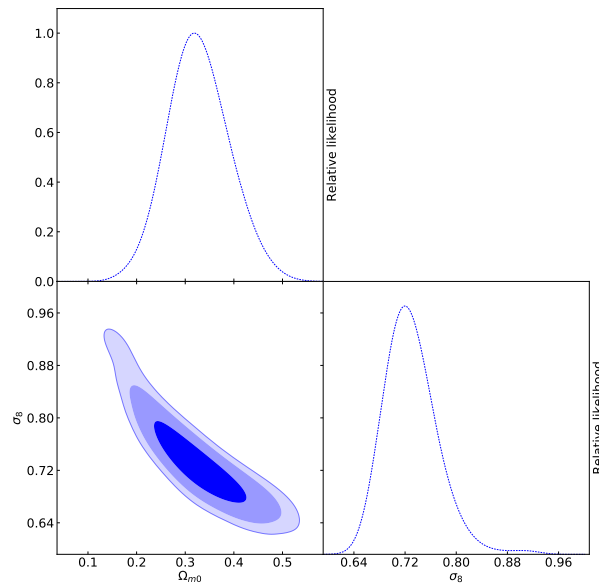
Figure 8: 1σ, 2σ and 3σ confidence regions as well as marginalized likelihood functions for cosmological parameters σ_8 and Ω_{m0} obtained from the MCMC analysis using the solely RSD data in the context of ΛCDM cosmology.
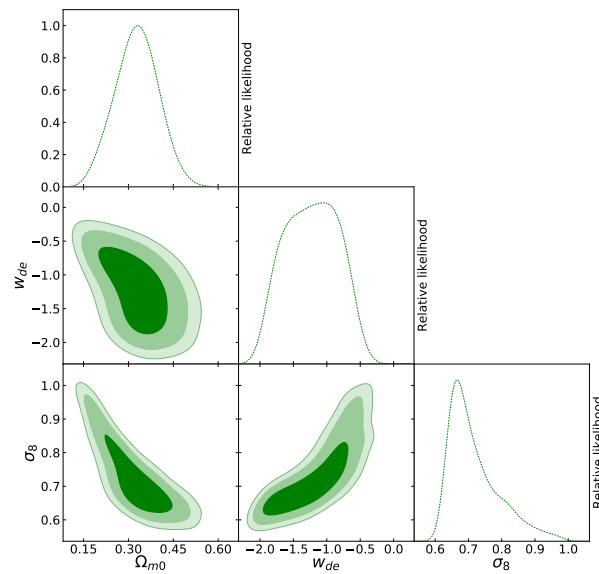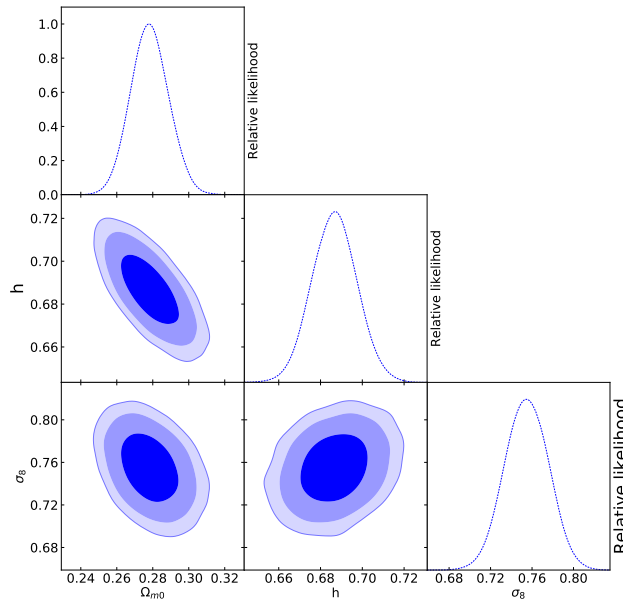

Figure 9: 1σ, 2σ and 3σ confidence regions as well as marginalized likelihood functions for cosmological parameters σ_8, w_{de} and Ω_{m0} obtained from the MCMC analysis using the solely RSD data in the context of wCDM cosmology.

Figure 10: 1σ, 2σ and 3σ confidence regions as well as marginalized likelihood functions for cosmological parameters σ_8, h, and Ω_{m0} obtained from the MCMC analysis using the combined expansion and RSD data in the context of ΛCDM cosmology.
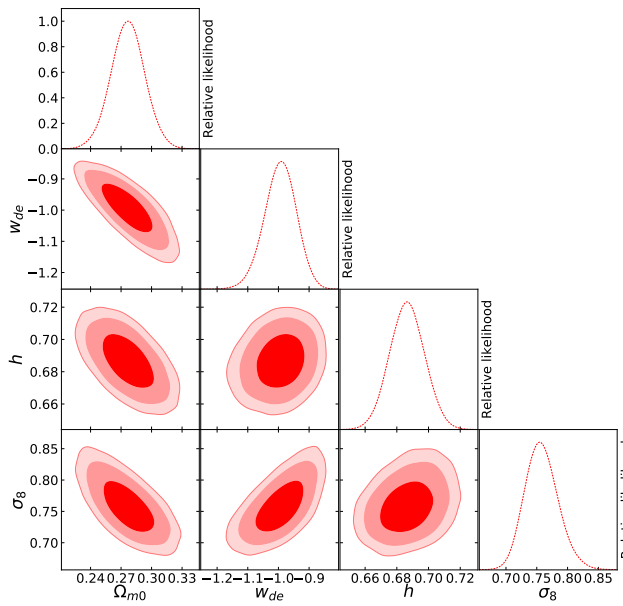

Figure 11: 1σ, 2σ and 3σ confidence regions as well as marginalized likelihood functions for cosmological parameters σ_8, h, w_{de}, and Ω_{m0} obtained from the MCMC analysis using the combined expansion and RSD data in the context of wCDM cosmology.
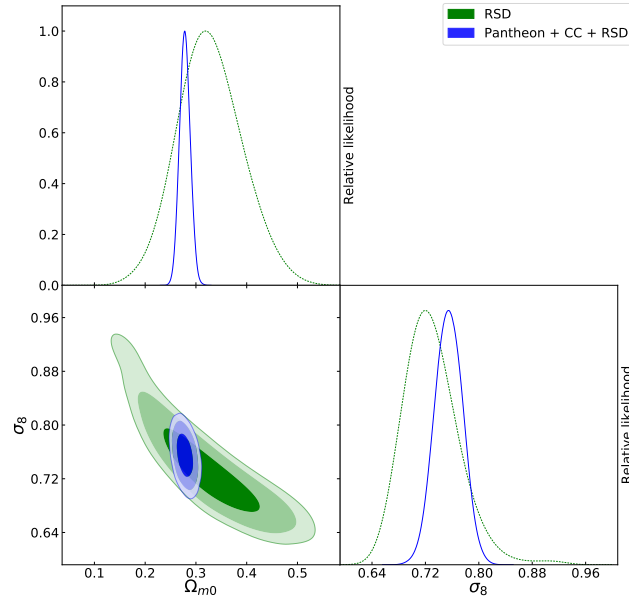
Figure 12: 1σ, 2σ and 3σ confidence regions as well as marginalized likelihood functions for cosmological parameters σ_8 and Ω_{m0} obtained from the MCMC analysis using the solely RSD (green) and combined expansion with RSD data (blue) in the context of ΛCDM cosmology.
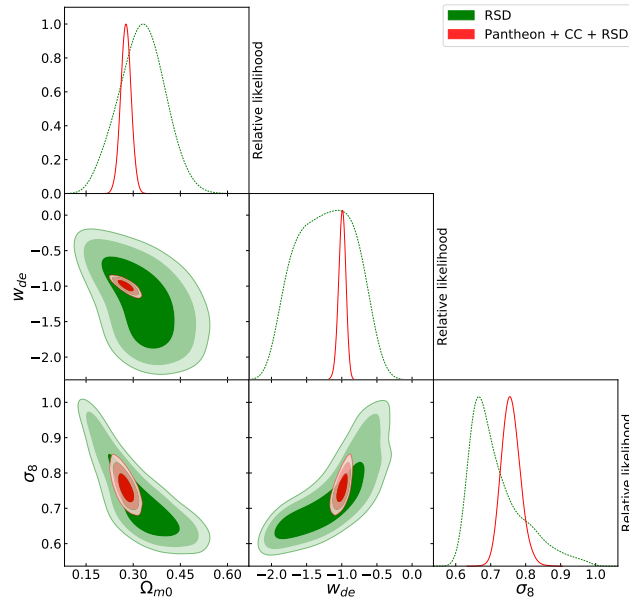

Figure 13: 1σ, 2σ and 3σ confidence regions as well as marginalized likelihood functions for cosmological parameters σ_8, w_{de} and Ω_{m0} obtained from the MCMC analysis using the solely RSD (green) and combined expansion with RSD data (red) in the context of wCDM cosmology.
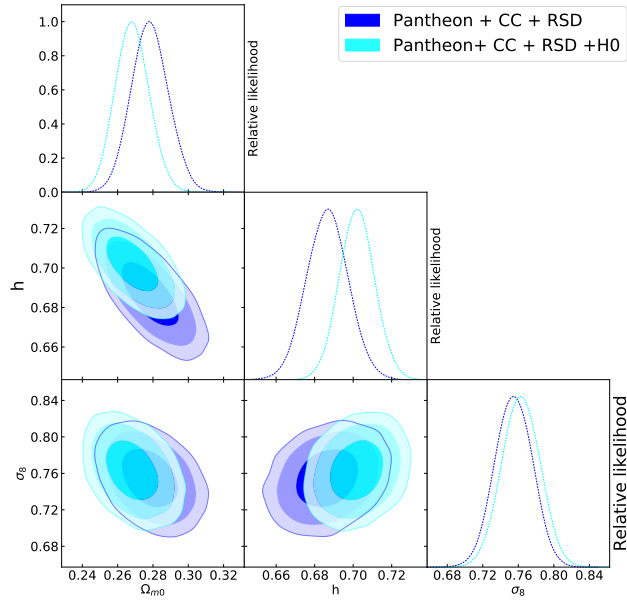
Figure 14: The comparison between confidence regions and marginalized likelihood functions of cosmological parameters σ_8, h, and Ω_{m0} for ΛCDM cosmology obtained from the MCMC analysis with (blue) and without (cyan) inclusion of H_0 data point.

Figure 15: The comparison between confidence regions and marginalized likelihood functions of cosmological parameters σ_8, h, w_{de}, and Ω_{m0} for wCDM cosmology obtained from the MCMC analysis with (red) and without (gray) inclusion of H_0 data point.

Figure 16: The comparison between confidence regions and marginalized likelihood functions of cosmological parameters σ_8, h, and Ω_{m0} for ΛCDM cosmology obtained from the MCMC analysis with (black) and without (blue) inclusion of BAO measurements.
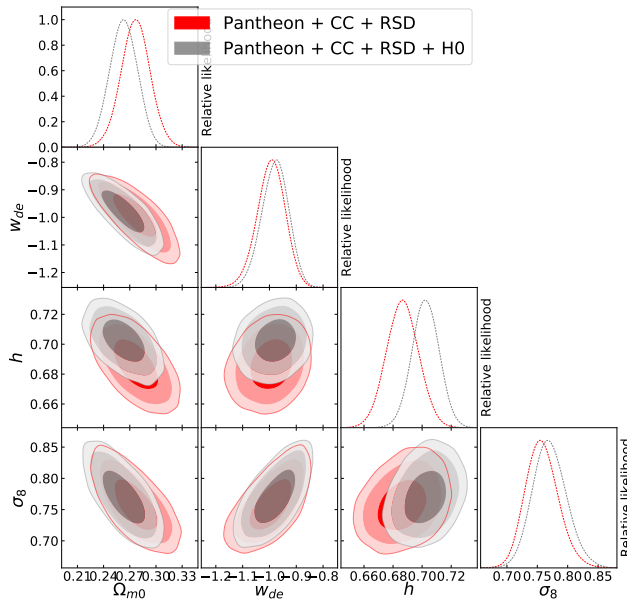

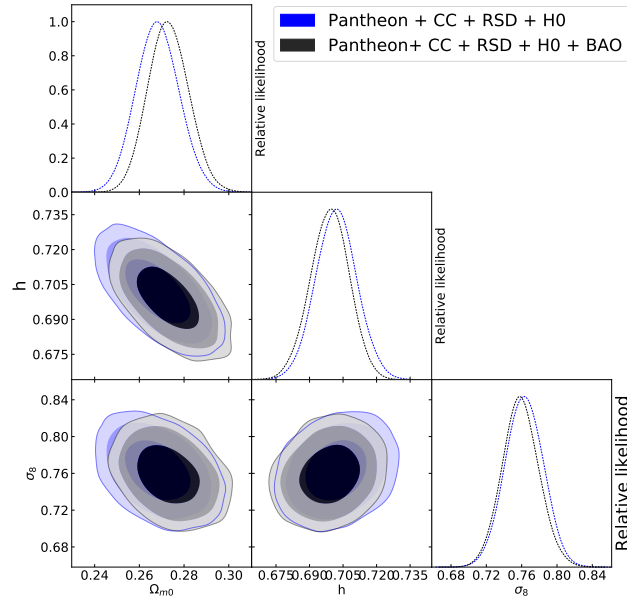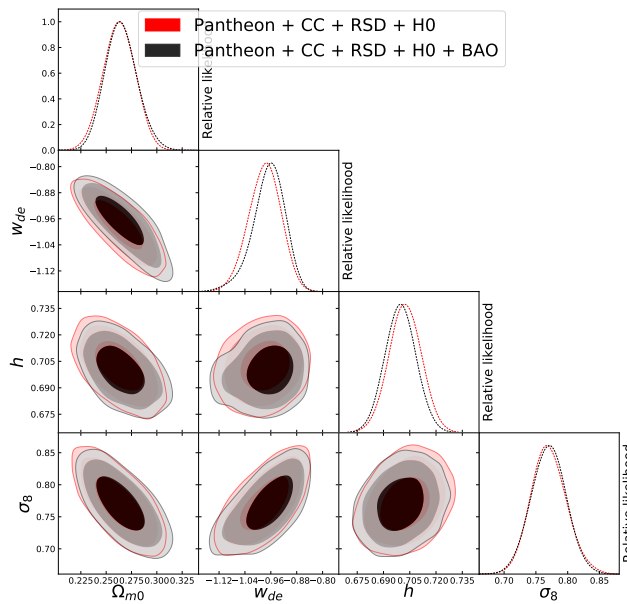
Figure 17: The comparison between confidence regions and marginalized likelihood functions of cosmological parameters σ_8, h, w_{de}, and Ω_{m0} for wCDM cosmology obtained from the MCMC analysis with (black) and without (blue) inclusion of BAO measurements.

Table 6: Best fit values of the matter density, Ω_{m0}, EoS parameter of DE, w_{de}, and dimensionless Hubble constant, h, obtained from the MCMC analysis using the Pantheon Supernova data combined with the CC data in Table 1.

Model	Ω_{m0}	w_{de}	h
ΛCDM	$0.277^{+0.011,+0.021,+0.028}_{-0.011,-0.021,-0.027}$	-1.00	$0.687^{+0.011,+0.022,+0.029}_{-0.011,-0.021,-0.028}$
wCDM	$0.275^{+0.017,+0.035,+0.046}_{-0.017,-0.033,-0.042}$	$-0.991^{+0.056,+0.097,+0.12}_{-0.047,-0.11,-0.15}$	$0.688^{+0.011,+0.022,0.029}_{-0.011,-0.022,-0.029}$

quantity $\frac{1}{\Delta\Omega_{m0}\Delta w_{de}}$ for different 1σ, 2σ and 3σ confidence regions. The results for Pantheon sample are ~ 50.7, ~ 13 & ~ 7.7, respectively for 1σ, 2σ and 3σ confidence regions . While these values are ~ 15.3, ~ 4.3 & ~ 2.5 for Union 2.1 and ~ 18.7, ~ 4.2 & ~ 2.05 for the Gold sample catalog. The best fit values of the parameters Ω_{m0} and w_{de} and their 1σ, 2σ and 3σ confidence regions are presented in Table. (5).

4.2 SnIa + CC data

In the previous section, we showed how increasing the data points of SnIa from early Gold sample data to current Pantheon catalog can tight the confidence regions of cosmological parameters. In this section, we combine the SnIa data with the CC data, $H(z)$, to show that one can get tighter regions of confidence level by using the different data from various observational catalogs. To do this, we combine the SnIa data from Pantheon catalog with the CC data from Table 1. We consider the standard ΛCDM and wCDM model and apply the MCMC analysis to obtain the best fit values and confidence regions of the cosmological parameters. The results are shown in Figures (6) and (7), respectively, for concordance ΛCDM and wCDM models. The numerical results are also shown in Table (6). Comparing the results from those of the Table (5), we conclude that combining the Pantheon SnIa data with the CC data changes slightly the confidence regions for both concordance ΛCDM and wCDM cosmologies. In fact, we expect that adding the CC data predicts more precise measurements of the cosmological parameters. In the case of ΛCDM model, the best fit value of Ω_{m0} obtained from Pantheon + CC constraint is roughly 0.8% lower than that of the Pantheon constraint only. So that the difference, in this case, is negligible. In the case of wCDM, the constraint value of Ω_{m0} obtained from Pantheon + CC sample is approximately 7% lower than that of the Pantheon constraint only. We observe that the best fit value of EoS parameter resulted from Pantheon + CC is -0.991 confirming the concordance ΛCDM moel even in 1σ error (see Table 6). Notice that we can not achieve this result by using the Pantheon sample only (see Table 5). One can also observe that the confidence regions for EoS parameter, w_{de} resulted from Pantheon + CC constraint is tighter than that of the Pantheon constrain only (see Tables 5 and 6). The other cosmological parameter that we constraint using the Pantheon + CC samples is the dimensionless Hubble constant h. We observe that, in this case, the ΛCDM and wCDM models are consistent with each other even in 1σ level.

4.3 RSD data

We now extend our analysis in the perturbation level. We mention that up to now our MCMC analysis is based on the expansion data including different SnIa samples and CC data extracted from cosmic chronometers. Here we constrain the properties of DE using the only RSD data. In the context of MCMC analysis and using the RSD data from Table 2, we constraint the cosmological parameter of both the ΛCDM and wCDM models. The

confidence regions and the likelihood functions for ΛCDM and wCDM models are depicted in Figures (8) and (9), respectively. The numerical results for both models are presented in Table (7). We observe that the best fit value of matter density Ω_{m0} obtained from the analysis based on RSD data is roughly 15% larger than that of the analysis based on the Pantheon+ CC data. We also see that the uncertainties of Ω_{m0} is much larger than that of the MCMC analysis based on the SnIa and SnIa + CC experiments. This result is expected, because the number of data extracted from RSD experiments is much lower than the data of SnIa and SnIa + CC analysis.

Table 7: Best fit values of matter density, Ω_{m0}, EoS parameter of DE, w_{de}, and mass variance within $8Mpch^{-1}$, σ_8, obtained from MCMC analysis using the RSD data in Table 2.

Model	Ω_{m0}	w_{de}	σ_8
ΛCDM	$0.327^{+0.060,+0.13,+0.17}_{-0.068,-0.12,-0.17}$	-1.00	$0.730^{+0.033,+0.085,+0.17}_{-0.047,-0.080,-0.089}$
wCDM	$0.328^{+0.073,+0.14,+0.18}_{-0.073,-0.15,-0.17}$	$-1.22^{+0.4,+0.70,+0.86}_{-0.4,-0.71,-0.86}$	$0.717^{+0.034,+0.17,+0.24}_{-0.092,-0.11,-0.12}$

Table 8: Best fit values of matter density, Ω_{m0}, EoS parameter of DE, w_{de}, dimensionless Hubble constant, h, and mass variance within $8Mpch^{-1}$, σ_8, obtained from MCMC analysis using the combination of Pantheon + CC datasets with RSD data.

Model	Ω_{m0}	w_{de}	h	σ_8
ΛCDM	$0.278^{+0.011,+0.021,+0.028}_{-0.011,-0.020,-0.026}$	-1.00	$0.687^{+0.011,+0.021,+0.028}_{-0.011,-0.021,-0.028}$	$0.755^{+0.021,+0.041,+0.053}_{-0.021,-0.041,-0.055}$
wCDM	$0.277^{+0.017,+0.033,+0.043}_{-0.017,-0.033,-0.044}$	$-0.994^{+0.054,+0.10,+0.13}_{-0.049,-0.11,-0.15}$	$0.687^{+0.011,+0.022,0.029}_{-0.011,-0.021,-0.028}$	$0.758^{+0.024,+0.055,+0.079}_{-0.029,-0.052,-0.065}$

Table 9: Best fit values of the matter density, Ω_{m0}, EoS parameter of DE, w_{de}, and dimensionless Hubble constant, h, obtained from the MCMC analysis using the Pantheon + CC + RSD data combined with the local measurement of H_0.

Model	Ω_{m0}	w_{de}	h	σ_8
ΛCDM	$0.2682^{+0.0097,+0.019,+0.025}_{-0.0097,-0.019,-0.025}$	-1.00	$0.7020^{+0.0092,+0.018,+0.024}_{-0.0092,-0.018,-0.024}$	$0.763^{+0.021,+0.042,+0.055}_{-0.021,-0.042,-0.055}$
wCDM	$0.263^{+0.016,+0.030,+0.040}_{-0.016,-0.031,-0.041}$	$-0.979^{+0.050,+0.10,+0.12}_{-0.050,-0.10,-0.13}$	$0.7024^{+0.0094,+0.018,0.024}_{-0.0094,-0.019,-0.025}$	$0.770^{+0.026,+0.058,+0.077}_{-0.029,-0.052,-0.069}$

4.4 SnIa + CC + RSD data

Here, we combine the expansion data including those of Pantheon and CC data with the RSD data in cluster level. The confidence regions and likelihood functions for the cosmological parameters of ΛCDM and wCDM models are shown in Figures (10) and (11), respectively. The best fit values and 1, 2 and 3σ errors of cosmological parameters are also reported in Table (8). Combining the expansion and RSD data, we get tighter constraints compare to previous analysis based on the solely RSD data. In particular, we show the confidence regions of the cosmological parameters obtained from MCMC analysis using (i) the RSD data and (ii) the Pantheon + CC + RSD data in Figures (12) and (13), respectively, for ΛCDM

Table 10: Best fit values of the matter density, Ω_{m0}, EoS parameter of DE, w_{de}, and dimensionless Hubble constant, h, obtained from the MCMC analysis using the Pantheon + CC + RSD + H_0 data combined with the measurement of BAO dataset.

Model	Ω_{m0}	w_{de}	h	σ_8
ΛCDM	$0.2730^{+0.0091,+0.018,+0.024}_{-0.0091,-0.017,-0.022}$	-1.00	$0.6991^{+0.0087,+0.017,+0.022}_{-0.0087,-0.018,-0.023}$	$0.759^{+0.021,+0.043,+0.056}_{-0.021,-0.040,-0.053}$
wCDM	$0.265^{+0.015,+0.044,+0.029}_{-0.017,-0.029,-0.036}$	$-0.966^{+0.054,+0.096,+0.10}_{-0.042,-0.10,-0.16}$	$0.6997^{+0.0090,+0.018,+0.023}_{-0.0090,-0.017,-0.023}$	$0.770^{+0.028,+0.054,+0.071}_{-0.028,-0.054,-0.072}$

and wCDM cosmologies. One can see that including the expansion results tighter constraint on the cosmological parameters for both ΛCDM and wCDM cosmologies. Quantitatively, we compute $\frac{1}{\Delta\Omega_{m0}\Delta\sigma_8}$ in the case of ΛCDM cosmology and $\frac{1}{\Delta\Omega_{m0}\Delta\sigma_8}$, $\frac{1}{\Delta\Omega_{m0}\Delta w_{de}}$, $\frac{1}{\Delta w_{de}\Delta\sigma_8}$ in the case of wCDM Universe. In ΛCDM cosmology, the quantity $\frac{1}{\Delta\Omega_{m0}\Delta\sigma_8}$, respectively in 1σ, 2σ and 3σ uncertainties are roughly 390, 97 and 42, by using the solely RSD data. While these values for Pantheon + CC + RSD data are roughly 4329, 1161 and 685, respectively. We observe that the these values for 1σ, 2σ and 3σ uncertainties obtained from Pantheon + CC + RSD data are respectively 11, 11 and 16 times larger than that of those values using the RSD data. This result shows that we can put more tighter constraints on the cosmological parameters using the low redshift expansion data compared to RSD data. The data in perturbation scales are not sufficient to put reasonable constraints on the cosmological parameters. Notice that this result is also due to the large error bars of the RSD observational data. We now repeat our analysis for wCDM cosmology. Within 1σ, 2σ and 3σ confidence regions and using the solely RSD data, we obtain (217, 49, 31), (34, 10, 7) and (40, 10, 6), respectively for quantities $\frac{1}{\Delta\Omega_{m0}\Delta\sigma_8}$, $\frac{1}{\Delta\Omega_{m0}\Delta w_{de}}$, $\frac{1}{\Delta w_{de}\Delta\sigma_8}$. While these values for Pantheon + CC + RSD are roughly (2219, 566, 319), (1142, 288, 164) and (732, 178, 99),respectively. We observe that in the case of $\frac{1}{\Delta\Omega_{m0}\Delta\sigma_8}$, the result for all 1σ, 2σ and 3σ regions obtained from Pantheon + CC + RSD data are approximately 10 times larger than the result obtained from RSD data. In the case of $\frac{1}{\Delta\Omega_{m0}\Delta w_{de}}$ ($\frac{1}{\Delta w_{de}\Delta\sigma_8}$), this value for Pantheon + CC + RSD data is approximately 30 (18) times larger than that of the RSD data. Hence, in agreement with the results of the ΛCDM cosmology, this prediction shows that in the case of wCDM model, we can also put tighter constraints on the cosmological parameters using the combined low redshift expansion and RSD data.

5   Combined data with H_0 and BAO measurements

In this section, we first add the local observational value of H_0 data point to the observational datasets used in the previous section to see that how including the H_0 data changes the results of our analysis. In the next step, we combine the observational datasets with that of the BAO data points and observe the effect of BAO measurements in our results.

5.1 H_0 data point

Combining the local value $H_0 = 73.48^{+1.66}_{-1.66}$ Km/s/Mpc [51] with the other low-redshift data including Pantheon, CC and RSD, we repeat our MCMC analysis for both ΛCDM and wCDM models. The numerical results of our statistical analysis is presented in Table(9). We also compare the confidence regions and marginalized likelihood functions of the cosmological parameters obtained from the analysis with and without H_0 in Figures (14) and (15), respectively, for ΛCDM and wCDM cosmologies (see also Tables 8 and 9). Without includ-

ing the H_0 data point (Table 8), we observe that the best fit values of h for both ΛCDM and wCDM models are roughly 2% larger than Planck inferred value and approximately 6% smaller than the local value of Hubble constant H_0. We see that by combining the H_0 data with other low redshift observational data (Pantheon + CC + RSD), the best fit value of h is 0.702 which is translated to $H_0 = 70.2$. Hence, our analysis based on Pantheon + CC +RSD + H_0 yields the lower tension between the low-redshift observational data and high redshift CMB experiments for Hubble constant. Numerically, we observe that the tension is alleviated from high value 3.4σ to low value $\sim 1.7\sigma$ (note that we consider $1\sigma = 1.66$ from $H_0 = 73.48^{+1.66}_{-1.66}$ Km/s/Mpc [51]). We would like to mention that our results presented in Tables (8) and (9) indicate no tension even in 1σ error between the best fit values of other cosmological parameters obtained from the analysis with and without H_0 (see also Figures 14 and 15).

5.2   BAO measurements

Here, we add the BAO data to Pantheon + CC + RSD + H_0 data points to perform an overall likelihood analysis and see the effect of including the BAO experiments in our analysis. Based on the equations (10,11,12 and 13), we can calculate the theoretical value of $d(z)$ and use the observational values in Table (3) to obtain the first χ^2 function for BAO as follows

$$\chi^2_{\text{bao},1} = \sum_i \frac{[d_{obs}(z_i) - d_{the}(z_i)]^2}{\sigma_i^2} \ , \tag{15}$$

In the next step, we calculate the second χ^2 function for BAO using the data points presented in Table (4). Notice that these data points are uncorrelated, except for the WiggleZ subset. The second χ^2 function reads

$$\chi^2_{\text{bao},2} = \sum_i \frac{[\alpha^*_{obs}(z_i) - \alpha^*_{the}(z_i)]^2}{\sigma_i^2}, \tag{16}$$

where $\alpha^*_{the} = d^{-1}(z) \times r_s^{fid}$ is calculated from equation (10.) It is emphasized that in equation (16), we do not consider the WiggleZ data points. Also in order to calculate α^*_{the} we use the values for r_s^{fid} presented in the last column of Table (4). Finally, we compute the third χ^2 function for WiggleZ subset as

$$\chi^2_{\text{bao},3} = \{\alpha^*_{obs}(z_i) - \alpha^*_{the}(z_i)\}\Sigma^{-1}_{\text{bao},ij}\{\alpha^*_{obs}(z_j) - \alpha^*_{the}(z_j)\} \ , \tag{17}$$

where α^*_{obs} and its corresponding redshift have been shown in WiggleZ subset of Table (4). The inverse of related covariance matrix Σ^{-1} is given by

$$\Sigma^{-1}_{WiggleZ} = \begin{pmatrix} 0.000217899 & -0.000111633 & 0.0000469829 \\ -0.000111633 & 0.000170712 & -0.00007184472 \\ 0.0000469829 & -0.0000718472 & 0.000165283 \end{pmatrix} . \tag{18}$$

The total χ^2_{bao} is then given by $\chi^2_{total} = \chi^2_{bao1} + \chi^2_{bao2} + \chi^2_{bao3}$. We now combine the BAO observations with Pantheon + CC + RSD + H_0 and perform an overall likelihood analysis on the basis of MCMC method for ΛCDM and wCDM cosmologies. Our results are showed in Table (10 as well as in Figures (16) and (17). As expected, adding the BAO data causes the tighter constraints of the cosmological parameters. Specifically, in the case of ΛCDM cosmology, tighter constraints on the cosmological parameters have been achieved (see Figure 16). Quantitatively speaking, we see that the constraint on Ω_{m0} and h parameters is

approximately $7 - 8\%$ tighter when we combine Pantheon + CC + RSD + H_0 data with BAO data points. While the differences between our analysis with and without BAO observations is negligible for the parameter σ_8. Comparing the results of Tables (9) and (10) shows that the constraints on the cosmological parameters with and without using the BAO data are consistent with each other within 1σ error. This result is valid for both ΛCDM and wCDM cosmologies.

6 Conclusion

In this work, we studied the properties of DE cosmologies by implementing the statistical analysis based on the MCMC technique. We use the low-redshift observational data including the SNIa data from the Gold sample, Union 2.1 and Pantheon catalogs as well as the CC data extracted from cosmic chronometers, the growth rate data extracted from RSD measurements, local measurement on H_0 data point and finally BAO dataset. We assumed the well-known ΛCDM and wCDM models as the DE cosmologies in our analysis. Our main conclusion of this work are presented as follows:

(i) First, we compared the results of the MCMC analysis for different Gold sample, Union 2.1 and Pantheon catalogs. We showed that in the case of Pantheon catalog, one can put tighter confidence regions on the cosmological parameters compare to the Gold sample and Union 2.1 catalogs. In particular, the confidence regions obtained from Pantheon sample are roughly three times smaller than those of the Gold sample data. This result is valid for both ΛCDM and wCDM cosmologies.

(ii) In the second step, we combined the Pantheon and CC data and obtained the confidence regions of the cosmological parameters. We concluded that in this case, the tighter constraints can be achieved compare than the case of Pantheon sample alone. While in the case of Pantheon data, the EoS parameter of DE deviates from the ΛCDM within 1σ error (see Table 5), we showed that by combining the Pantheon and CC data the EoS parameter of DE for wCDM model is well consistent with the ΛCDM universe within 1σ level (see Table 6).

(iii) In the third step, we studied the properties of DE in cluster scales using the RSD observational data. We obtained the large uncertainties of cosmological parameters using the growth rate data alone (see Table 7). The large uncertainties obtained here is due to this fact that the number of RSD observational data is much lower compare to Pantheon data. The other important thing that causes the big uncertainties of cosmological parameters is the large error bars of the RSD observational data. Then, by combining Pantheon + CC with RSD data, we observed tighter constraints and small uncertainties of cosmological parameters compare to results of RSD data alone (see Table 8 and Figures 12 and 13).

(iv) In the fourth step, we combined the Pantheon + CC + RSD datasets with that of the local measurement of Hubble constant H_0. While the local value of $H_0 = 73.48^{+1.66}_{-1.66}$ Km/s/Mpc [51] has a big $\sim 3.4\sigma$ tension with CMB inferred value [52] $H_0 = 67.4^{+0.5}_{-0.5}$Km/s/Mpc, the combination of local value H_0 with other low-redshifts Pantheon + CC + RSD data yields $H_0 = 70.2$ (see Figures 14 and 15 as well as Table 9). This means that in our analysis the high tension $\sim 3.4\sigma$ with high redshift CMB observations is alleviated to $\sim 1.7\sigma$ by assuming the Pantheon + CC + RSD + H_0 datasets.

(v) In the fifth step, we implemented an overall likelihood analysis by combining Pantheon + CC + RSD + H_0 with BAO datasets. We concluded that by including the BAO observational data into account, the constraints on the matter density Ω_{m0} and dimensionless Hubble constant h for ΛCDM cosmology are approximately $7-8\%$ tighter than the analysis without BAO dataset (see Figure 16 and Table 10). However, the constraints with and without including the BAO data are consistent with each other within 1σ error.

Authors' Contributions

The author contributed to data analysis, drafting, and revising of the paper and agreed to be responsible for all aspects of this work.

Data Availability

No data available.

Conflicts of Interest

The author declares that there is no conflict of interest.

Ethical Considerations

The author has diligently addressed ethical concerns, such as informed consent, plagiarism, data fabrication, misconduct, falsification, double publication, redundancy, submission, and other related matters.

Funding

This research did not receive any grant from funding agencies in the public, commercial, or non profit sectors.

References

[1] Riess, A. G., Strolger, L. G., Tonry, J., Casertano, S., & et al. 2004, ApJ, 607, 665.

[2] Riess, A. G., Strolger, L. G., Casertano, S., Ferguson, H. C., & et al. 2007, ApJ, 659, 98.

[3] Perlmutter, S., & et al. 1998, Nature, 391, 51.

[4] Perlmutter, S., Aldering, G., Goldhaber, G., & et al. 1999, ApJ, 517, 565.

[5] Bennett, C. L., & et al. 2003, ApJS, 148, 1.

[6] Spergel, D. N., & et al. 2003, ApJS, 148, 175.

[7] Spergel, D. N., & et al. 2007, ApJS, 170, 377.

[8] Eisenstein, D. J., Zehavi, I. D., Hogg, W., & et al. 2005, ApJ, 633, 560.

[9] Hawkins, E., & et al. 2003, MNRAS, 346, 78.

[10] Tegmark, M., Strauss, M. A., Blanton, M. R., & et al. 2004, PRD, 69, 103501.

[11] Close, S., & et al. 2005, MNRAS, 362, 505.

[12] Hamuy, H., & et al. 1996, Astron. J. 112, 2391.

[13] Conley, C. & et al. 2011, Astron. J. Suppl. 192, 1.

[14] Koyama, K. 2016, Reports on Progress in Physics, 79, 046902.

[15] Copeland, E. J., Sami, M., & Tsujikawa, S., 2006, IJMPD, D15, 1753.

[16] Weinberg, S. 1981, Reviews of Modern Physics, 61, 1.

[17] Caldwell, R. R., Dave, R., & Paul J. 1998, PRL, 80, 1582.

[18] Adam G., & et al. 2004, ApJ, 607, 665.

[19] Tonry, J. L., & et al. 2003, ApJ, 594, 1.

[20] Barris, B. J., & et al. 2004, ApJ, 602, 571.

[21] Suzuki, N., & et al. 2012, ApJ, 746, 85.

[22] Scolnic, D. M., & et al. 2018, ApJ, 859, 101.

[23] Malekjani, M., Basilakos, S., Davari, Z., & et al. 2017, MNRAS, 464, 1192.

[24] Batista, R. C., & Pace, F. 2013, JCAP1306, 044.

[25] Malekjani, M., Rezaei, M., & Akhlaghi, I. A. 2018, PRD, 98, 063533.

[26] Mehrabi, A., Malekjani, M., & Pace, F. 2015, Astrophys. Space Sci, 356, 129.

[27] Mehrabi, A., Basilakos, S., & Pace, F. 2015, MNRAS, 452, 2930.

[28] Mehrabi, A., Basilakos, S., Malekjani, M., & Davari, Z. 2015, PRD, 92, 123513.

[29] Basilakos, S., Plionis, M., & Sola, J. 2009, PRD, 80, 083511.

[30] Nesseris, S., Pantazis, G., & Perivolaropoulos, L. 2017, PRD, 96, 023542.

[31] Zhang, C., Zhang, H., Yuan, S., Zhang, T. J., & Sun, Y. 2014, Res. Astron. Astrophys., 14, 1221.

[32] Simon, J., Verde, L., & Jimenez, R. 2005, PRD, 71, 123001.

[33] Moresco, M., & et al. 2012, JCAP, 1208, 006.

[34] Chuang, C. H., & Wang, Y. 2012, MNRAS, 426, 226.

[35] Stern, D., Jimenez, R., Verde, L., Kamionkowski, M., & Stanford, S. A. 2010, JCAP, 1002, 008.

[36] Busca, N. G., & et al. 2013, Astron. Astrophys., 552, A96.

[37] Huterer, D., Shafer, D., Scolnic, D., & Schmidt, F. 2017, JCAP, 1705, 015.

[38] Beutler, F., & et al. 2011, MNRAS, 416, 3017.

[39] Padmanabhan, N., & et al. 2012, MNRAS, 427, 2132.

[40] Ross, A. J., Samushia, L., Howlett, C., Percival, W. J., & Manera, M. 2015, MNRAS, 449, 835.

[41] Anderson, L., & et al. 2014, MNRAS, 441, 21.

[42] Kazin, E. A., & et al. 2014, MNRAS, 441, 3524.

[43] Alam, S., & et al. 2017, MNRAS, 470, 2617.

[44] Jackson, J. C. 1972, MNRAS, 156, 1P.

[45] Rezaei, M., Malekjani, M., Basilakos, S., Mehrabi, A., & Mota, D. F. 2017, ApJ, 843, 65.

[46] Baghram, S., & Rahvar, S. 2010, JCAP, 1012, 008.

[47] Pace, F., Waizmann, J. C., & Bartelmann, M. 2010, MNRAS, 406, 1865.

[48] Pace, F., Moscardini, L., Crittenden, R., Bartelmann, M., & Pettorino, V. 2014, MN-RAS, 437, 547.

[49] Eisenstein, D. J. , Hu, W., 1998, ApJ, 496, 605.

[50] Hinshaw, G., & et al. 2013, ApJS, 208, 19.

[51] Riess, A. G., & et al. 2018, ApJ, 861, 126.

[52] Aghanim, N., & et al. 2018, A&A, 641, A6.

[53] Casertano, S., Riess, A. G., Bucciaelli, B., & Lattanzi, G. 2017, A&A, 599, A67.

[54] Suyu, S. H., & et al. 2017, MNRAS, 468, 2590.

[55] Bonvin, V., & et al. 2017, MNRAS, 465, 4914.

[56] Hastings, W. k. 1970, Biometrika, 57, 97.

[57] Biesiada, M., Godlowski, W., & Szydlowski, M. 2005, ApJ, 622, 28.